Plant Biotechnology Journal Open Access

Plant Biotechnology Journal (2022) **20**, pp. 1387–1401 doi: 10.1111/pbi.13821

Du13 encodes a C_2H_2 zinc-finger protein that regulates *Wx*^{b} pre-mRNA splicing and microRNA biogenesis in rice endosperm

Yue Cai[1,†], Wenwei Zhang[1,†], Yushuang Fu[1,†], Zhuangzhuang Shan[1,†], Jiahuan Xu[1], Peng Wang[1], Fei Kong[1], Jie Jin[1], Haigang Yan[1], Xinyuan Ge[1], Yongxiang Wang[1], Xiaoman You[1], Jie Chen[1], Xin Li[1], Weiwei Chen[1], Xingang Chen[1], Jing Ma[1], Xiaojie Tang[1], Jie Zhang[1], Yiqun Bao[3], Ling Jiang[1], Haiyang Wang[2] and Jianmin Wan[1,2,*]

[1]*State Key Laboratory for Crop Genetics and Germplasm Enhancement, Jiangsu Plant Gene Engineering Research Center, Nanjing Agricultural University, Nanjing, China*

[2]*National Key Facility for Crop Gene Resources and Genetic Improvement, Institute of Crop Science, Chinese Academy of Agricultural Sciences, Beijing, China*

[3]*College of Life Sciences, Nanjing Agricultural University, Nanjing, China*

Received 16 September 2020; revised 27 January 2022; accepted 10 March 2022.

**Correspondence* (Tel +86 25 84396516; fax +86 25 84396516; email: wanjm@njau.edu.cn)

[†]These authors contributed equally to this work.

Keywords: rice, dull endosperm, *OsGBSSI/Wx*, C_2H_2 zinc-finger protein, microRNA, pre-mRNA splicing.

Summary

Amylose content is a crucial physicochemical property responsible for the eating and cooking quality of rice (*Oryza sativa* L.) grain and is mainly controlled by the *Waxy* (*Wx*) gene. Previous studies have identified several *Dull* genes that modulate the expression of the *Wx*^{b} allele in *japonica* rice by affecting the splicing efficiency of the *Wx*^{b} pre-mRNA. Here, we uncover dual roles for a novel *Dull* gene in pre-mRNA splicing and microRNA processing. We isolated the *dull* mutant, *du13*, with a dull endosperm and low amylose content. Map-based cloning showed that *Du13* encodes a C_2H_2 zinc-finger protein. Du13 coordinates with the nuclear cap-binding complex to regulate the splicing of *Wx*^{b} transcripts in rice endosperm. Moreover, Du13 also regulates alternative splicing of other protein-coding transcripts and affects the biogenesis of a subset of microRNAs. Our results reveal an evolutionarily conserved link between pre-mRNA splicing and microRNA biogenesis in rice endosperm. Our findings also provide new insights into the functions of *Dull* genes in rice and expand our knowledge of microRNA biogenesis in monocots.

Introduction

Starch accounts for approximately 90% of the dry weight of rice grains, which constitute the primary food source consumed by over half of the world's population (Zeng *et al*., 2007). Two different kinds of starch, amylose and amylopectin, are deposited in the rice endosperm. Moreover, amylose content (AC) is the major determinant of the eating and cooking quality of rice. Thus, modifying AC is a major strategy for quality improvement in rice breeding (Kiswara *et al*., 2014).

AC in rice endosperm is determined by the major *Waxy* (*Wx*) locus and many minor loci, including more than a dozen *dull endosperm* loci, named *du1* to *du12(t)* (Aluko *et al*., 2004; Kiswara *et al*., 2014). The rice *Wx* locus encodes granule-bound starch synthase I (OsGBSSI), a key enzyme involved in amylose biosynthesis in rice endosperm (Wang *et al*., 1990). Rice cultivars carry two wild-type alleles at the *Wx* locus, *Wx*^{a} and *Wx*^{b}. *Wx*^{a} predominates in *O. sativa* spp. *indica* species with high AC and produces 10 times more OsGBSSI protein than *Wx*^{b}, which is mainly distributed in *japonica* cultivars with low or intermediate AC (Zeng *et al*., 2007). The lower abundance of OsGBSSI in *japonica* cultivars is due to decreased transcript levels of *Wx*^{b} caused by a G-to-T mutation at the splicing donor site of *Wx*^{b} intron 1, which diminishes its splicing efficiency and activates two cryptic splice donor sites within exon 1 (Cai *et al*., 1998; Frances *et al*., 1998; Hirano *et al*., 1998; Isshiki *et al*., 1998). The two splice sites show a weaker match to the 5′ consensus splice site sequence, leading to the lower splicing efficiency of *Wx*^{b} transcripts. However, *dull* mutations do not affect the splicing of the *Wx*^{a} transcripts with the normal splice donor site of intron 1 (Isshiki *et al*., 2000).

dull mutants exhibit an endosperm with a dull appearance and low AC that contrasts with the typical translucent endosperm of wild-type rice. Several *Dull* genes have been shown to modulate the splicing efficiency of *Wx*^{b} intron 1 (Isshiki *et al*., 2000, 2008). Although rice breeders have employed *dull* mutants to improve the eating and cooking quality of rice, only two *Dull* genes have been cloned to date. *Du1* encodes a member of the pre-mRNA processing protein (PRP) family and affects the splicing of *Wx*^{b} and starch biosynthesis (Zeng *et al*., 2007), while *Du3* encodes the mRNA cap-binding protein OsCBP20 that forms a heterodimeric cap-binding complex (OsCBC) with OsCBP80 (Isshiki *et al*., 2008). OsCBP20 might affect the transcription, splicing, and stability of *Wx*^{b} in rice endosperm (Isshiki *et al*., 2008).

The CBC can bind to the cap structure of transcripts produced by RNA polymerase II. In Arabidopsis (*Arabidopsis thaliana*), the CBC participates in the biogenesis of microRNAs (miRNAs) and splicing of cap-proximal introns in pre-mRNAs (Kim *et al*., 2008; Laubinger *et al*., 2008; Raczynska *et al*., 2009). The CBC coordinates its various roles with the C_2H_2 zinc-finger protein SERRATE (SE; Grigg *et al*., 2005; Laubinger *et al*., 2008; Raczynska *et al*., 2014). However, the exact functional relationship

© 2022 The Authors. *Plant Biotechnology Journal* published by Society for Experimental Biology and The Association of Applied Biologists and John Wiley & Sons Ltd. This is an open access article under the terms of the Creative Commons Attribution-NonCommercial-NoDerivs License, which permits use and distribution in any medium, provided the original work is properly cited, the use is non-commercial and no modifications or adaptations are made.

between SE and CBC in regulating miRNA biogenesis and RNA splicing has remained elusive.

In this study, we describe and characterize the novel rice *dull* mutant, *du13*. Map-based cloning revealed that the *Du13* gene encodes a C_2H_2 zinc-finger protein homologous to Arabidopsis SE. We determined that Du13 and OsCBC act together to regulate the splicing of Wx^b. We observed significant changes in the alternative splicing (AS) patterns of some genes in the *du13* mutant background. Du13 also affects the accumulation of a subset of miRNAs in rice endosperm. We thus documented here that the rice *Dull* gene, *Du13*, may be involved in the regulation of miRNA biosynthesis.

Results

Identification of *du13*

We identified the *du13* mutant from a mutant population of *japonica* cv. Koshihikari (Figure S1a) for its endosperm appearance between waxy (as in the *wx* mutant *w53* in the Koshihikari background) and translucent (wild-type Koshihikari; Figure 1a, b). Transverse sections of *du13* grains took on a reddish-brown colour upon iodine staining that is distinct from the dark-blue staining of wild-type grains and the light-brown staining of *w53* grains (Figure 1c). The AC of *du13* grains was 7.05%, compared to 16.77% in the wild-type (Figure 1d). Scanning electron microscopy (SEM) analysis showed that the *du13* endosperm consisted of tightly packed and polyhedron-shaped starch granules (SGs), as in the wild type (Figure S1b–g). We obtained similar results using semi-thin sections of developing endosperm (Figure S1h, i), but noticed small cavities within SGs in *du13* (Figure S1g), resembling those of previously reported *dull* mutants (Kaushik and Khush, 1991).

Compared to the wild type, the *du13* mutant showed a slower grain-filling rate, in accordance with smaller and lighter grains (Figure S1j–m; Table S1). *du13* plants also exhibited an increased plant height and panicle length, but a reduced tilling number (Figure S1a; Table S1). Collectively, these data showed that the *du13* mutation has pleiotropic effects on multiple plant phenotypes.

Altered starch physicochemical characteristics of the *du13* mutant

Total starch and protein contents were comparable between *du13* and wild-type grains (Figure S2a, b), whereas the lipid content of *du13* was almost twice that of the wild type (Figure S2c). In *du13* developing endosperm, AC was substantially lower at the onset of amylose biosynthesis, and this tendency continued until seed maturation (Figure S2d, e). We also determined the amylopectin chain-length distribution of *du13* endosperm starch. When compared to wild-type levels, the *du13* mutant had a lower proportion of short chains with a degree of polymerization (DP) in the range of 9–15, and a higher proportion of amylopectin chains with DP in the ranges of 6–8 and 16–33 (Figure S2f).

We also analysed the pasting properties of *du13* endosperm starch with a rapid visco analyzer (RVA). The viscosity profiles of *du13* and wild-type pasting starch followed a similar pattern, although that of *du13* maintained a lower level relative to the wildtype (Figure S2g). In addition, *du13* grains displayed higher values of peak viscosity and breakdown viscosity, but lower values for other RVA parameters when compared to the wild type (Table S2), indicating a relatively soft and elastic texture. We concluded that the *du13* mutant alters the physicochemical characteristics of the starch.

Map-based cloning of *Du13* and complementation of the *du13* mutant

For genetic analysis, we crossed the *du13* mutant to the parental cultivar Koshihikari. In the F_2 population, translucent to dull endosperm segregated with a ratio of about 3:1 ($n = 778$, $\chi^2 = 0.829 < \chi^2_{0.05,1} = 3.84$), indicating that *du13* is a single-gene recessive mutation.

We generated an F_2 segregating population derived from a cross between *du13* (*japonica*) and Nanjing 11 (*indica*) to map the *Du13* locus between simple sequence repeat (SSR) markers W26 and W6 on the long arm of chromosome 6 (Figure 2a). Subsequent fine-mapping narrowed down the candidate interval to a 187-kb region with 26 putative open reading frames (ORFs; Figure 2a). Sequence analysis revealed a C-to-T substitution at position 4482 in exon 8 of ORF 26 (*LOC_Os06g48530*) in the *du13* mutant (Figure 2b), introducing a premature stop codon in place of the wild-type Arg-333 residue (Figure S3).

To assess whether *LOC_Os06g48530* corresponds to the *Du13* gene, we introduced a construct consisting of the *LOC_Os06g48530* coding region, driven by the *UBIQUITIN* promoter, into the *du13* mutant background. Seeds harvested from three independent transgenic T_2 lines recovered their vitreous appearance (Figure 2c). Iodine staining of transverse-cut grains from these lines was also similar to that of the wild type (Figure 2c), as reflected by their similar amylose contents (Figure S4a). We failed to detect the protein encoded by *LOC_Os06g48530* in the *du13* mutant, while a protein of the appropriate molecular weight reappeared in the transgenic lines, using a specific antibody raised in rabbits (Figure 2d). For an independent confirmation, we introduced a CRISPR-Cas9 construct expressing a single guide RNA (sgRNA) targeting exon 8 of *LOC_Os06g48530* into Nipponbare to generate additional mutants in this gene. The sequencing of PCR amplicons of *LOC_Os06g48530* from the genomic DNA of transgenic plants identified knockout mutant Y6 with a 1-bp insertion in exon 8 (Figures 2b and S3a) that is predicted to produce a truncated polypeptide of only 490 amino acids instead of 723 in the wild type (Figures 2e and S3b). Relative to Nipponbare, Y6 produced visibly smaller seeds with dull endosperms, and their transverse sections stained reddish-brown with iodine, as observed in *du13* (Figure 2f). The AC of Y6 seeds also dramatically decreased from 16.26% in the wildtype to 5.00% (Figure 2g). We failed to detect the protein-encoded *LOC_Os06g48530* in the Y6 mutant by immunoblot analysis (Figure 2h). We obtained similar results with three other knockout mutants in the *japonica* cv. Ningjing 7 background (Figure S4b–d). Given that these knockout mutants shared the same phenotypes as Y6, we focused on the Y6 mutant chosen for further study. Together, these data demonstrated that *LOC_Os06g48530* is the *Du13* gene.

Du13 is a zinc-finger protein homologous to SE

The *Du13* gene contains 12 exons and encodes a protein with 723 amino acids that is predicted to harbour a putative nuclear localization signal at its N terminus, a domain of unknown function 3546 (DUF3546), and an Arsenite-resistance protein-2 (ARS2) domain near its C terminus (Figure 2b, e; http://smart.embl-heidelberg.de/; https://www.ncbi.nlm.nih.gov/protein/). The ARS2 domain included a single C_2H_2-type zinc finger, which

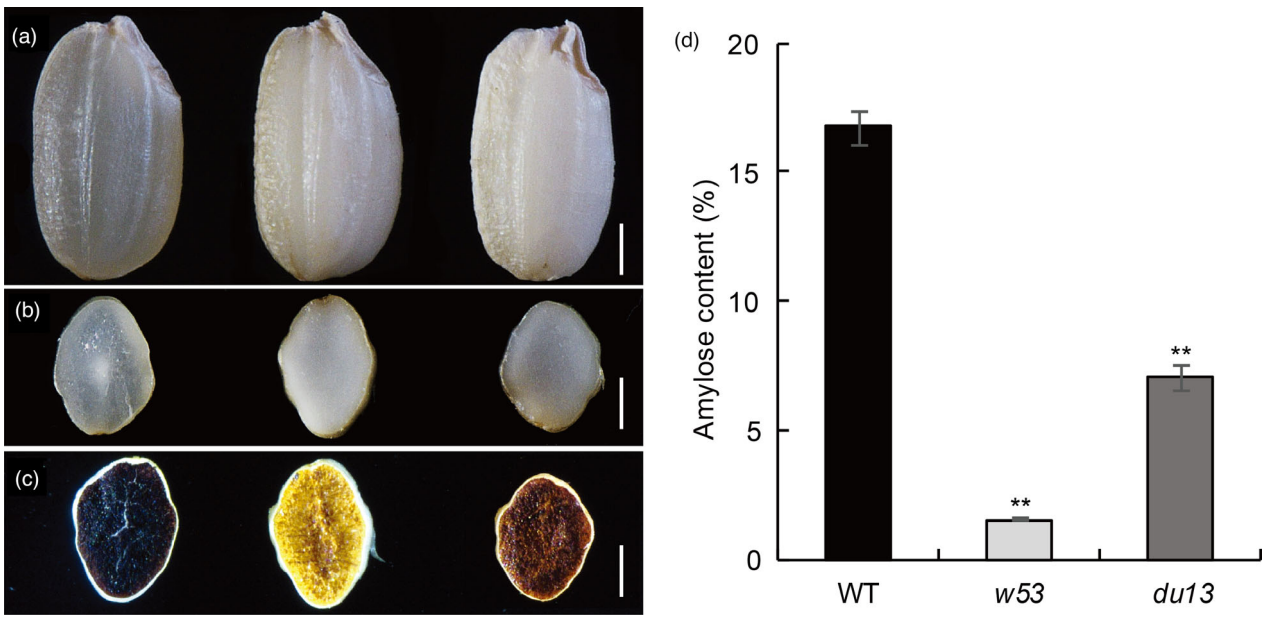

Figure 1 Phenotypic analysis of the *du13* mutant. (a–c) Phenotypes of wild-type (WT, Koshihikari, left), *w53* (a *waxy* mutant in the 'Koshihikari' genetic background, middle) and *du13* (right) grains. (a) Appearance of mature dehulled grains. (b) Transverse sections of mature grains. (c) Transverse sections stained with iodine. Bars, 1 mm. (d) Amylose contents of mature seeds of the WT, *w53* and *du13*. Values are means ± standard deviation (SD; $n = 3$). $*P < 0.05$, $**P < 0.01$, as determined by Student's *t*-test.

is a general feature of SE orthologues (Wilson *et al*., 2008; Figure 2e). In the *du13* and Y6 mutants, the truncated Du13 proteins would completely or partially lack the ARS2 domain, if they indeed accumulate in these mutants (Figure 2e).

To understand the phylogenetic relationship of Du13 and SE homologs in plants, we extracted the predicted protein sequences from phylogenetically different organisms (Figure S5a). Our phylogenetic analysis revealed that the rice genome encodes three distinct SE homologs; Du13, ZOS2-03 (*LOC_Os02g05610*) and ZOS8-11 (*LOC_Os08g40560*). The three rice SE orthologues clustered with SE-related proteins from purple false brome (*Brachypodium distachyon*). Du13 and ZOS2-03 share about 78% and 53% amino acid identity with SE, respectively, while ZOS8-11 shares the highest identity with SE at 85%. Interestingly, the monocots rice, purple false brome, and sorghum (*Sorghum bicolor*), have at least two *SE*-related genes, whereas there is only a single *SE* homolog in dicots such as Arabidopsis, soybean (*Glycine max*), and barrel clover (*Medicago truncatula*), as in mammals (Wilson *et al*., 2008). These putative SE orthologues harbour similar domains in the same relative order, suggesting a high degree of conservation (Figure S5b, c).

We determined the expression pattern of *Du13* using quantitative RT-PCR (qRT-PCR). We detected *Du13* expression in seedlings, young roots, leaves, leaf sheaths, culms, panicles, and mature roots, with the highest level being seen in leaves (Figure S6a). In developing seeds, *Du13* expression peaked at an early stage (approximately 3 days after fertilization [DAF]) and then gradually declined (Figure S6b), thus echoing the results of immunoblot analysis (Figure S6c). In the *du13* mutant, *Du13* expression was remarkably lower than in the wild type (Figures 2d and S6d). These results indicate that *Du13* is constitutively expressed in all tested tissues, and that the largest increase in *Du13* expression in the grain coincides with the initiation stage of grain development (Wang *et al*., 2013).

We transiently transfected a *35S-Du13-GFP* construct in rice protoplasts, expressing a fusion between *Du13* and the green fluorescent protein (*GFP*) under the control of the cauliflower mosaic virus (CaMV) 35S promoter. The Du13-GFP fusion protein localized to the nucleus, while the free GFP control was widely distributed in the cytoplasm (Figure S6e). The mutation in *du13* had no effect on Du13 subcellular localization (Figure S7).

Du13 affects splicing of the Wx^b pre-mRNA in rice endosperm

As the *Wx* gene is predominantly expressed in endosperm and pollen (Isshiki *et al*., 2000), we investigated whether the *du13* mutant also affected amylose biosynthesis in pollen. Iodine staining showed that wild-type and *du13* pollens are comparable in their appearance (Figure 3a, b). We conclude that the *du13* mutant differentially influences the expression of *Wx* in endosperm and pollen.

Compared to the wild type, OsGBSSI accumulated to remarkably lower levels in the endosperms of *du13* and the knockout mutant Y6 (Figures 2h and 3c). In agreement, OsGBSSI activity also decreased dramatically in *du13* and Y6 developing endosperms, compared to their respective wild type and a *du13* complemented line (Figure 3d). qRT-PCR analysis showed no significant changes in the levels of *Wx* transcript between *du13* and the wild type or the complemented line, or between Nipponbare and Y6 (Figure 3e). We then examined the splicing efficiency of Wx^b intron 1 in *du13* and Y6 endosperm. As illustrated in Figure 3f, two cryptic splice sites can be activated in the Wx^b pre-mRNA, with one site (site 2) located 93 nucleotides upstream of the normal splicing site and the second site (site 1) one base upstream of the normal site. As Wx^b transcripts spliced from the normal site or the second cryptic site are indistinguishable by RT-PCR, these two sites are collectively called site 1 (Isshiki *et al*., 2008). qRT-PCR analysis showed that

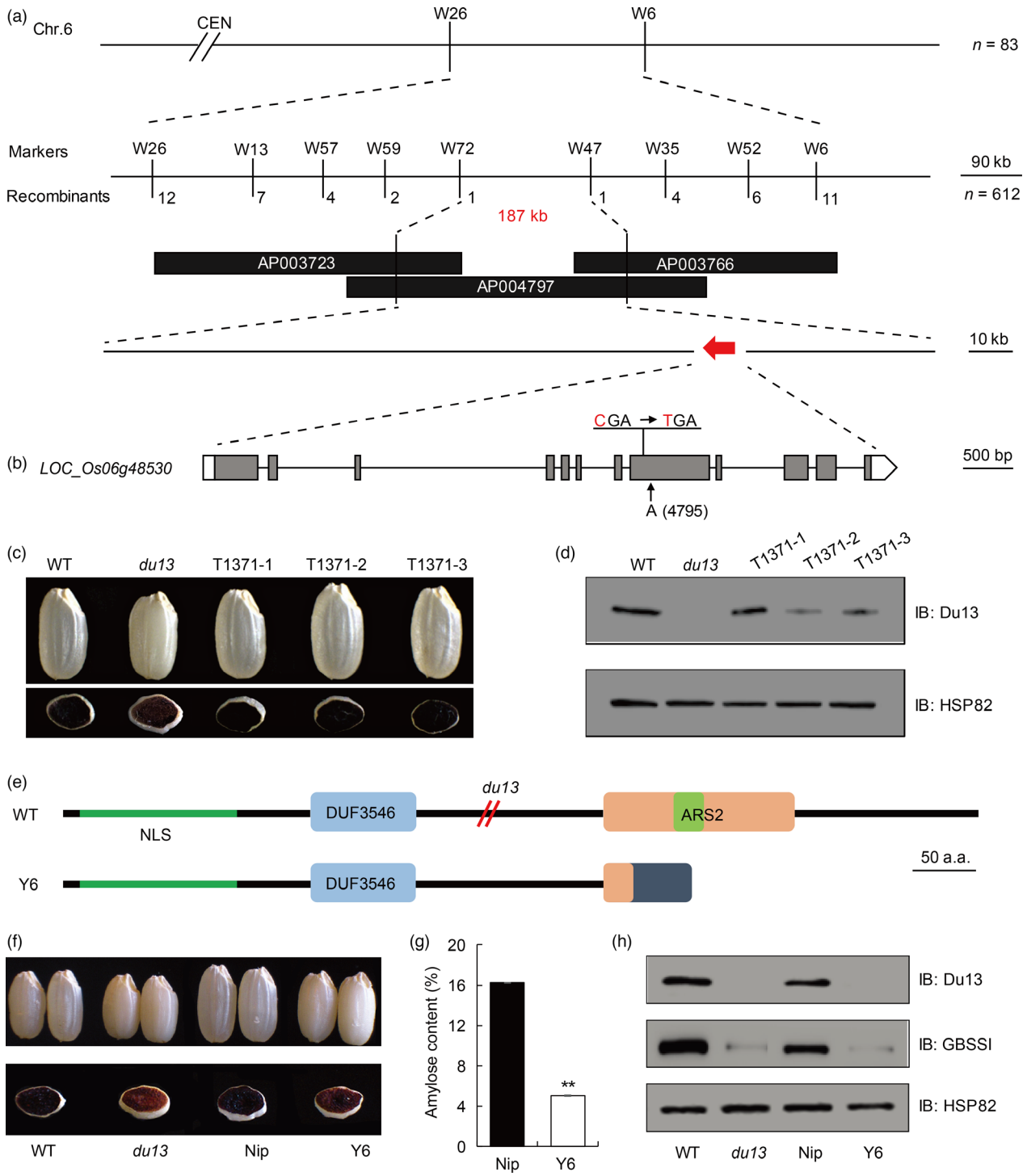

Figure 2 Map-based cloning and complementation of *Du13*. (a) Fine-mapping of the *Du13* locus. The molecular markers and the numbers of recombinants are indicated. CEN, centromere. (b) Structure of the *Du13* locus and positions of the mutations in *du13* and the *Du13*-knockout mutant Y6. A single nucleotide substitution in *du13* generated a premature stop codon, while an additional nucleotide A (4795) was inserted in Y6. (c) Functional complementation of the *du13* mutant with *LOC_Os06g48530* restored a normal grain appearance in three independent transgenic lines (T1371-1, –2, and –3, upper panel). Lower panel, transverse seed sections stained with iodine. (d) Immunoblot analysis of Du13 protein abundance in mature seeds of the wild type (WT), *du13*, and three transgenic lines. (e) Schematic diagram of the functional domains present in Du13. Nuclear localization signal, NLS, green line; DUF3546 domain, blue box; ARS2 domain, orange box, containing a C_2H_2 zinc finger (green box). Double red slashes indicate the approximate location of the premature stop codon in *du13*. a.a., amino acids. (f) Mature seeds of the WT, *du13*, Nip, and Y6 (upper panel). Lower panel, transverse seed sections stained with iodine. (g) Amylose contents of Nip and Y6 seeds. (h) Immunoblot analysis of Du13 and OsGBSSI in mature seeds of the WT, *du13*, Nip, and Y6. Anti-HSP82 antibodies were used as a loading control in (d) and (h). Nip, Nipponbare; IB, immunoblotting.

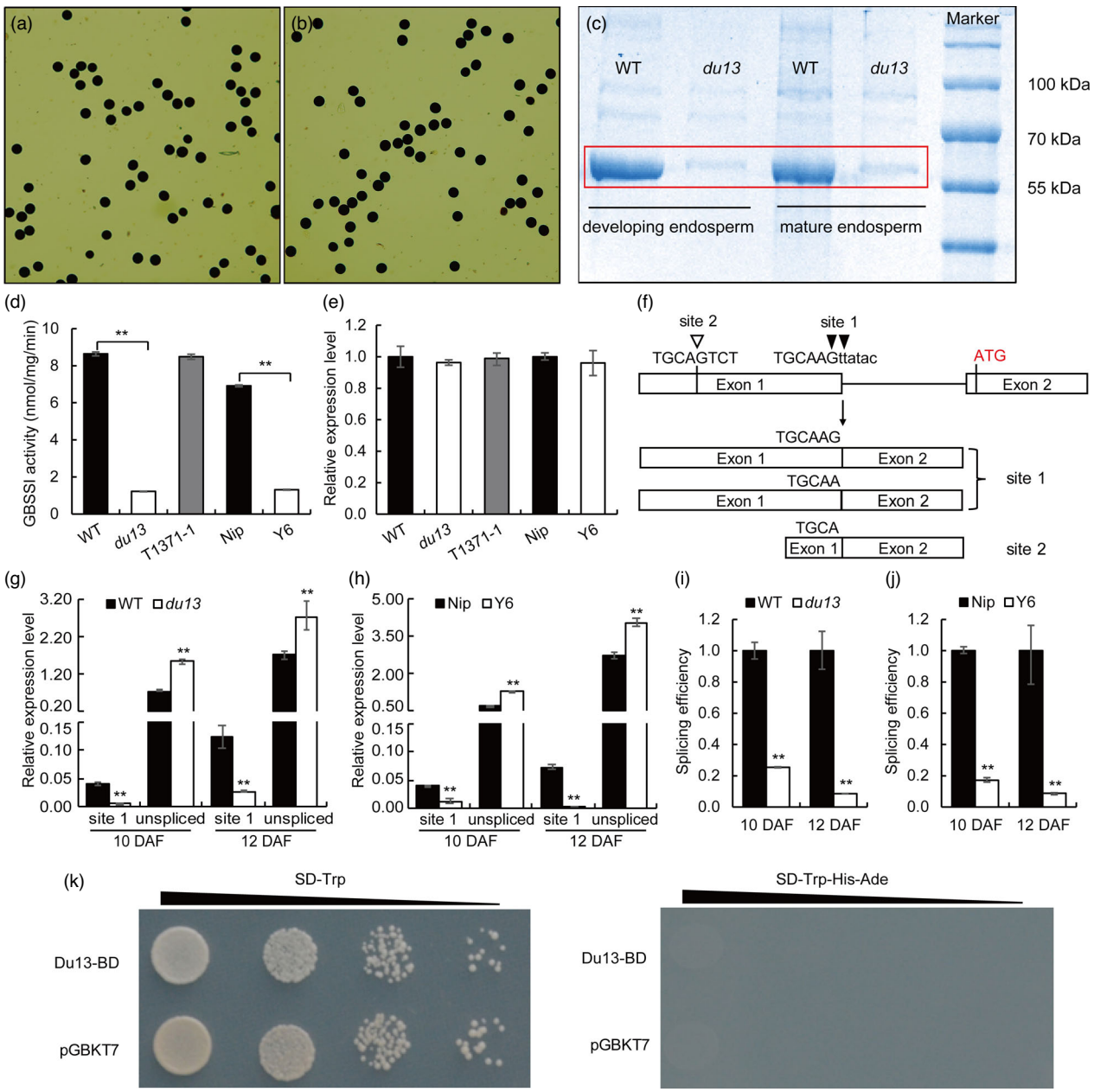

Figure 3 Loss of *Du13* function affects the splicing of *Wx*^{b} in rice endosperm. (a, b) Pollen grains of the wild type (WT, a) and *du13* (b) stained with iodine. (c) SDS-PAGE analysis of OsGBSSI abundance in WT and *du13* developing endosperm at 10 days after fertilization (DAF) or in mature endosperm. OsGBSSI is inside the red frame. The protein was extracted from developing or mature endosperms as described previously (Liu *et al.*, 2009). (d, e) OsGBSSI activity (d) and *OsGBSSI* expression levels (e) in developing endosperms from the WT, *du13*, the representative complemented line T1371-1, Nip, and Y6 at 10 DAF. The levels of *OsGBSSI* in the WT and Nip were set to 1 in (e). (f) Schematic diagram of the possible splicing patterns of the *Wx*^{b} pre-mRNA. (g, h) qRT-PCR analysis of *Wx*^{b} transcripts spliced at site 1 in developing endosperms of the WT and *du13* (g), or Nip and Y6 (h) at 10 and 12 DAF. The levels of *Wx*^{b} transcripts in the WT and Nip were set to 1. (i, j) qRT-PCR analysis of *Wx*^{b} splicing efficiency in developing endosperms of the WT and *du13* (i), or Nip and Y6 (j) at 10 and 12 DAF. The splicing efficiency of *Wx*^{b} was calculated as previously described (Zhang *et al.*, 2014a); WT or Nip values were set to 1. Values are means ± SD ($n = 3$). $^*P < 0.05$, $^{**}P < 0.01$, as determined by Student's *t*-test between the WT and mutant. *Actin I* was used as an internal control in (e, g–j). Nip, Nipponbare. (k) Du13 does not have transcription activity.

the abundance of *Wx*^{b} transcripts spliced at site 1 was much lower in *du13* and Y6 developing endosperms at 10 and 12 DAF compared to the wild type, concomitantly with a stark increase in unspliced *Wx*^{b} levels (Figure 3g, h). Indeed, the splicing efficiency of *Wx*^{b} transcripts in *du13* dropped to approximately one-third and one-tenth of the wild type in developing endosperm at 10 and 12 DAF, respectively, similar to that in Y6 (Figure 3i, j). Therefore, loss of Du13 function impaired splicing of *Wx*^{b} transcripts in rice endosperm.

The *du13* mutation also affected the expression of several starch biosynthesis-related genes (Figure S8), which might explain the altered fine structure of amylopectin in *du13* (Figure S2f). We

tested whether Du13 exerted direct transactivation activity in yeast cells by fusing Du13 to the DNA binding domain of the transcription factor GAL4, but observed no transactivation activity (Figure 3k). Therefore, the altered expression levels of starch biosynthetic genes in *du13*, might result from indirect effects of the *du13* mutation.

Functional analysis of Du13 in transient assays using rice protoplasts

To explore the effects of Du13 on the splicing of Wx^b, we used a transient assay system in rice protoplasts and the Wx^b-*gus* (*β-glucuronidase*) reporter construct for the analysis of splicing (Figure 4a). Co-transfection of rice protoplasts with the Wx^b-*gus* reporter and the *35S-Du13* cDNA construct elevated GUS activity approximately three-fold relative to the control (Figure 4b). By contrast, GUS activity was much lower in *du13* protoplasts relative to wild-type protoplasts upon transfection with the Wx^b-*gus* reporter (Figure 4c).

We also examined the effects of Du13 on splicing efficiency and splice site selection of Wx^b-*gus*. In protoplasts transfected with the Wx^b-*gus* reporter, site 1 was preferentially used (Figure 4d). However, when Wx^b-*gus* was co-transfected with *35S-Du13*, Wx^b-*gus* transcripts showed a strong increase in preference for splicing at site 1 together with a slight increase at site 2, indicating enhanced splicing efficiency (Figure 4d). Co-transfection of Wx^b-*gus* with *35S-du13* largely abolished Wx^b-*gus* splicing though slightly increased the GUS activity (Figure 4b, d). Moreover, only site 2 appeared to be selected at the 5′ splice site by du13 (Figure 4d).

In developing endosperms from the *du13* and Y6 mutants and their respective wild-type cultivars, site 1 was preferentially used (Figure 4e, f). The *du13* mutant also exhibited a lower splicing efficiency of Wx^b, which progressively decreased over the course of endosperm development (Figure 4e), consistent with the results of Figure 3i. We observed a similar trend in the Y6 mutant (Figures 3h, j, 4f). Notably, unspliced transcripts of Wx^b-*gus* accumulated to lower levels in protoplasts co-transfected with *35S-Du13*, but highly accumulated when co-transfected with *35S-du13* (Figure 4d). We noticed similar effects in developing endosperms (Figure 4e, f), in agreement with the qRT-PCR results (Figure 3g, h).

Du13 interacts with OsCBC and splicing factors

The *du13* mutant had a similar dull endosperm phenotype as *du3*, carrying a mutation in OsCBP20 (Isshiki *et al.*, 2008), prompting us to hypothesize that Du13 and OsCBC might work together to regulate Wx^b splicing. We thus examined the potential for physical interactions between Du13 and OsCBC subunits.

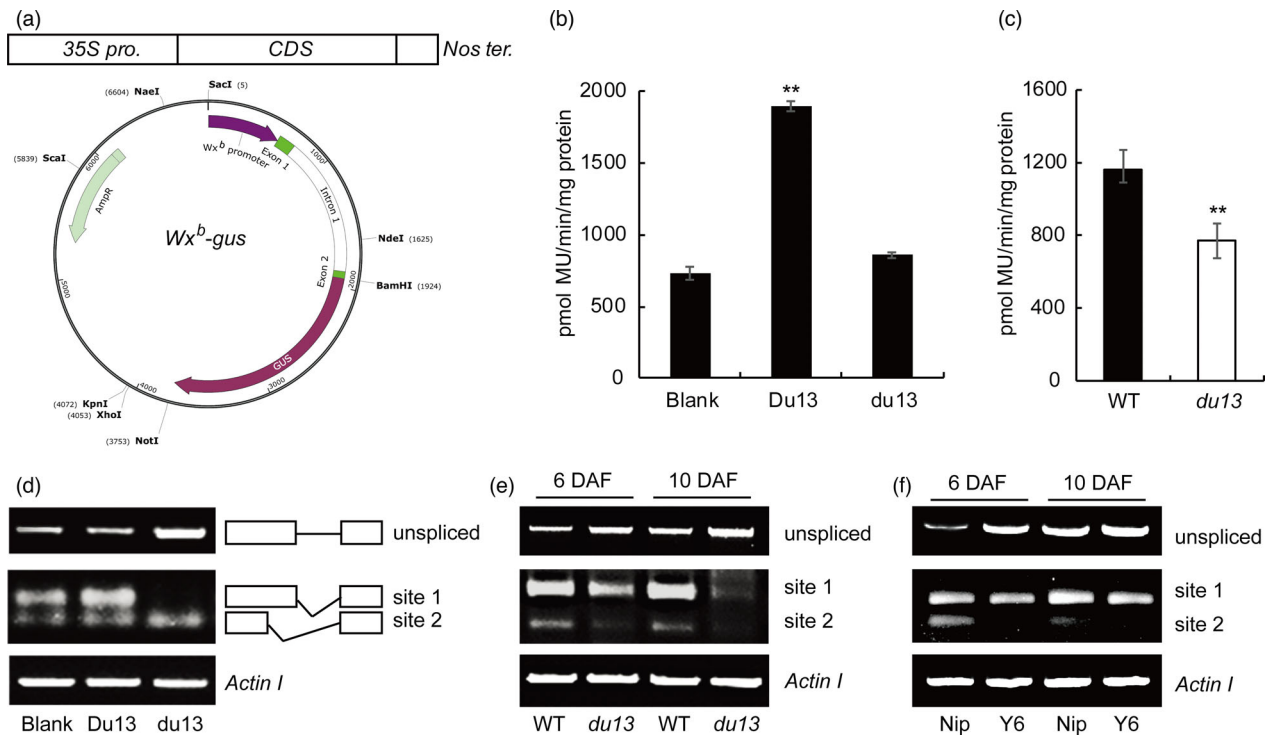

Figure 4 Effects of Du13 on GUS activity derived from the Wx^b-*gus* reporter. (a) Schematic diagrams of constructs for transfection assays. The Wx^b-*gus* reporter harbours the Wx^b promoter, exon 1, intron 1, and part of exon 2 from Wx^b with the ATG codon, cloned in-frame and upstream of the *Gus* reporter gene. The cDNAs of *Du13* and *du13* were placed under the control of the CaMV 35S promoter. If the expressed protein stimulates the splicing of intron 1 in Wx^b-*gus*, GUS activity will increase (Isshiki *et al.*, 2006). (b) GUS activity in co-transfected protoplasts. The *35S-Du13* and *35S-du13* constructs were co-transfected into protoplasts with the Wx^b-*gus* construct. Ten micrograms each of Wx^b-*gus* and *35S-Du13* or *35S-du13* plasmid DNA was added to 5×10^6 protoplasts. Values are means ± SD (n = 3). (c) GUS activity in wild-type (WT) and *du13* protoplasts transfected with Wx^b-*gus*. Values are means ± SD (n = 3). $^*P < 0.05$, $^{**}P < 0.01$, as determined by Student's t-test. (d) Effects of *35S-Du13* and *35S-du13* on the splicing of Wx^b intron 1 in protoplasts. The top gel shows unspliced Wx^b-*gus* transcripts. The middle gel shows transcripts spliced at site 1 (top fragments) or site 2 (bottom fragments) from Wx^b-*gus*. The bottom gel shows the internal control *Actin I*. (e) Splicing pattern of Wx^b intron 1 in WT and *du13* developing endosperm at 6 and 10 DAF. (f) Splicing pattern of Wx^b intron 1 in Nip and Y6 developing endosperm at 6 and 10 DAF. *Actin I* was used as an internal control in (e) and (f). Nip, Nipponbare.

We analysed the subcellular localization of OsCBP20 and OsCBP80 in *Nicotiana benthamiana* leaves. OsCBP20 showed a clear nuclear localization, while OsCBP80 localized to the cytoplasm and the nucleus (Figure S7). OsCBP20 accumulated in the nucleoplasm as well as in nuclear speckles. These two rice proteins, therefore, displayed the same localization pattern as their *Arabidopsis* counterparts (Kierzkowski *et al.*, 2009). A bimolecular fluorescence complementation (BiFC) assay indicated that OsCBP20 interacted with OsCBP80 in nuclear speckles (Figure S9a). BiFC assays also demonstrated physical interaction between Du13 and the OsCBC subunits OsCBP20 and OsCBP80 (Figure 5a). We observed a strong and homogenous fluorescence signal from reconstituted enhanced yellow fluorescent protein (eYFP) in the nuclei of cells co-infiltrated with *Du13* and *OsCBP80* constructs, but predominantly in nuclear speckles of cells co-infiltrated with *Du13* and *OsCBP20* constructs (Figure 5a). An *in vivo* co-immunoprecipitation (Co-IP) assay also confirmed that OsCBP20 and OsCBP80 could be co-immunoprecipitated by Du13 in total *N. benthamiana* leaf extracts (Figure 5b). Together, our results indicated that both OsCBC subunits form a complex with Du13 in the nucleus. Interestingly, like *OsGBSSI*, *OsCBP20* and *OsCBP80* expression peaked during the middle stage of grain development (Figure S9b–d), when a rapid increase in starch accumulation and seed weight occurs (Wang *et al.*, 2013). We observed no significant changes in the expression of *OsCBP20* or *OsCBP80* in *du13* endosperm (Figure S9e, f).

We detected no interactions between Du1 and Du13 or between Du1 and OsCBC using yeast two-hybrid (Y2H) and BiFC assays (Figure S10). By contrast, Du13 interacted with the four Ser/Arg-rich (SR) splicing factors RSp29, RSZp23, and two homologs of RSZp23 (Figures S7 and S11). RSp29 and RSZp23 were previously shown to affect Wx^b splicing (Isshiki *et al.*, 2006). The N terminus of Du13 mediated these interactions (Figure S11c).

Du13 is involved in alternative splicing of genome-wide rice genes

We examined whether alternative splicing (AS) was affected in *du13* through transcriptome deep sequencing (mRNA-seq). In wild-type endosperm, we detected a high frequency of the alternative 3′ splice site (40.44%), followed by the alternative 5′ splice site (22.98%), exon skipping (21.33%), intron retention (13.10%), and mutually exclusive exon choice (2.15%; Figure 6a). In *du13* endosperm, the frequency of AS events changed, for alternative 3′ or 5′ splice sites (35.97% and 19.71%, respectively), exon skipping (23.42%), intron retention (17.80%), and mutually exclusive exon (3.10%; Figure 6a; Table S3). These results thus suggested that AS at the alternative 3′ splice site occurs more frequently than at the 5′ splice site in plants, in agreement with a previous study (Raczynska *et al.*, 2014). When looking at the distribution of different AS events within introns, we noticed that intron retention AS events increased in the first and last introns or genes with a single intron in the *du13* mutant (Figure 6b), while AS at alternative 5′ and 3′ splice sites increased greatly in the first intron (Figure 6c, d).

To confirm a regulatory role for Du13 in AS of rice gene transcripts, we characterized AS of several mRNAs by RT-PCR with intron-flanking primers. We detected higher levels of unspliced transcripts accumulating in *du13* compared to the wild type (Figure 6e), potentially reflecting an effect on general splicing efficiency in the *du13* mutant and confirming a role for Du13 as a regulator of AS of gene transcripts in rice.

Du13 participates in miRNA processing

We tested whether Du13 might also affect the accumulation of mature miRNAs. A subset of miRNAs accumulated to lower levels in *du13* compared to the wild type, as determined by miRNA-seq analysis (Table S4). In agreement, the target genes of these miRNAs largely exhibited higher transcript levels (Table S4). We

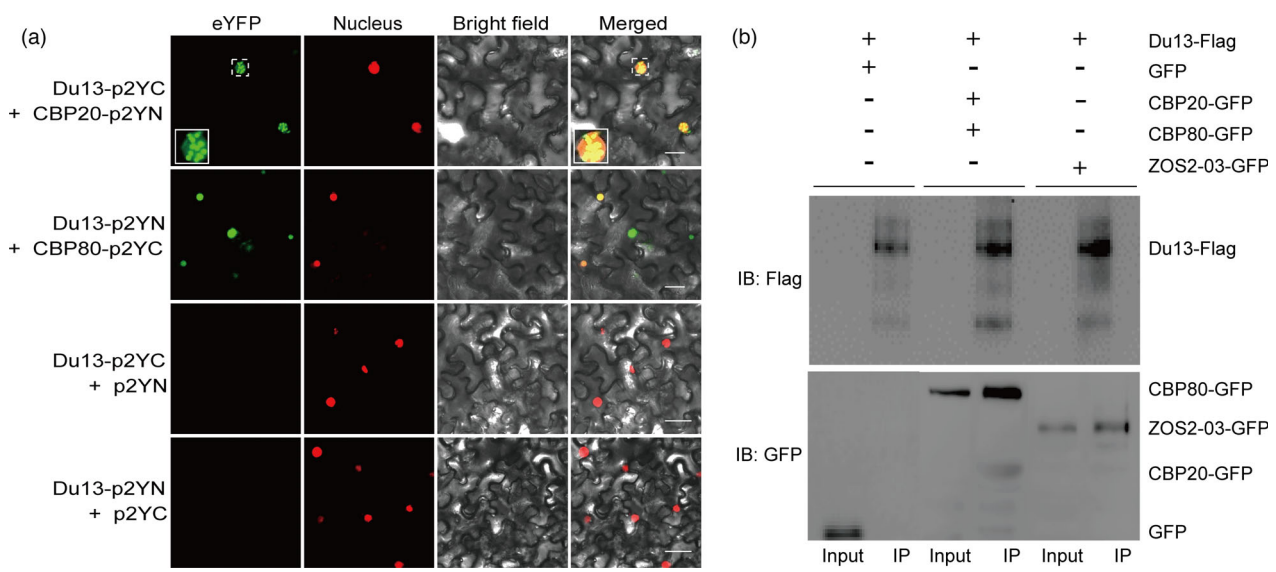

Figure 5 Du13 interacts with OsCBC. (a) BiFC assays showing that Du13 interacts with OsCBC in the nucleus of *N. benthamiana* leaf cells. The insets are magnified views of a representative nucleus in the dotted rectangles. OsMADS3-mCherry was used as a nuclear marker. Bars, 20 μm. (b) Co-IP assays showing that OsCBP20-GFP, OsCBP80-GFP, and ZOS2-03-GFP co-immunoprecipitate with Du13-Flag in total *N. benthamiana* leaf extracts with anti-Flag antibodies. IB, immunoblotting.

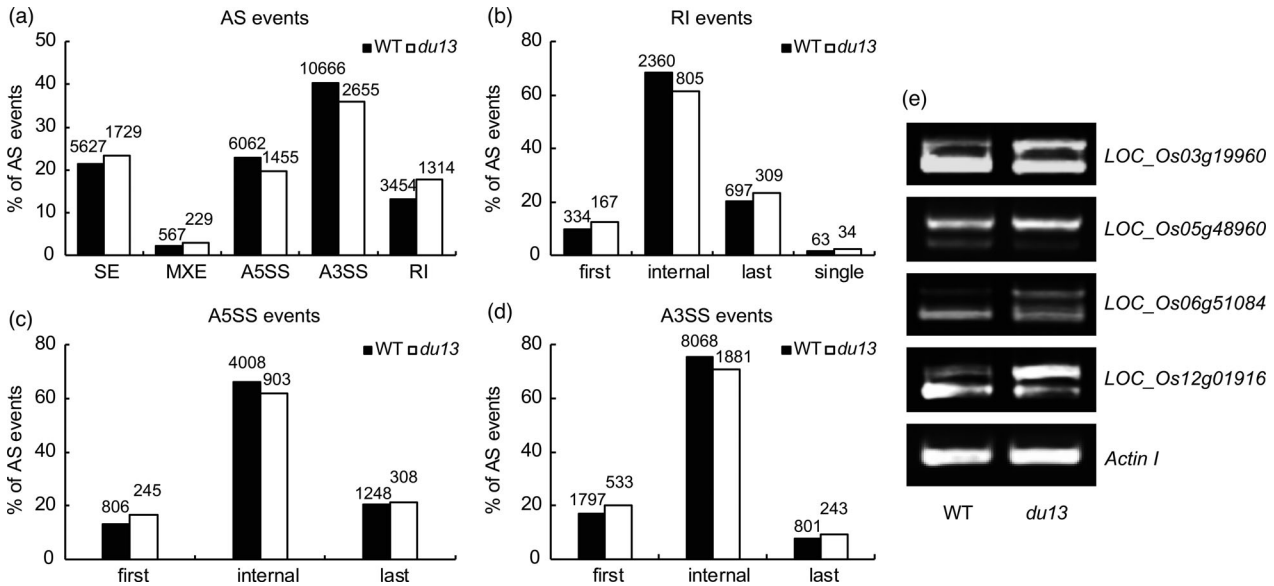

Figure 6 Distribution of changed alternative splicing (AS) events in the wild type (WT) and the *du13* mutant. (a) Distribution of alternatively spliced events: skipped exon (SE), mutually exclusive exon (MXE), alternative 5′ splice site (A5SS), alternative 3′ splice site (A3SS), retained intron (RI) in the WT and *du13*. (b–d) Distribution of RI (b), A5SS (c), and A3SS (d) events within first introns, internal introns, last introns or genes containing a single intron (b). Numbers above bars indicate the number of AS events. (e) Validation of RI in selected genes by conventional RT-PCR analysis. *LOC_Os03g19960* encodes an ATP-dependent RNA helicase; *LOC_Os05g48960* encodes a U2AF splicing factor; *LOC_Os06g51084* encodes starch branching enzyme I (BEI); *LOC_Os12g01916* encodes Double-stranded RNA-binding motif containing protein-2 (DRB-2/ DRB1-2).

used qRT-PCR analyses to validate the altered expression of these miRNAs in *du13*. The levels of osa-miR435, osa-miR444e, osa-miR1866-3p, osa-miR5144-5p, and osa-miR5794 were dramatically reduced in *du13* and Y6 compared to their respective wild-type cultivars (Figures 7a and S12a). The levels of osa-miR1850.2 were slightly reduced in *du13* (Figure 7a), but markedly reduced in Y6 (Figure S12a). These results were largely in agreement with the miRNA-seq analysis (Table S4). Intriguingly, only a subset of intron-less pri-miRNAs were affected in *du13* (http://structuralbiology.cau.edu.cn/cgi-bin/hgGateway?hgsid=3390&clade=plant&org=Nipponbare_v7&db=0). We further examined the expression levels of miRNA biogenesis components in *du13* but observed no substantial differences in their expression between *du13* and the wild type (Figure S9g).

We examined pri-miRNA transcript levels in *du13* and Y6 endosperms by semi-quantitative RT-PCR to test whether the *du13* and Y6 mutants lowered primary miRNA (pri-miRNA) levels or the processing efficiency of the pri-miRNA transcripts. The pri-miRNA transcripts of less abundant miRNAs in *du13* and Y6 accumulated to higher levels compared to their respective wild types (Figures 7b and S12b), indicating less effective processing of pri-miRNAs. By contrast, pri-miRNA transcripts of upregulated miRNAs in *du13* and Y6 displayed a decreased abundance, while we saw no obvious changes for the pri-miRNA transcripts of a slightly reduced miRNA in *du13* (Figures 7b and S12b). As miRNAs negatively regulate the abundance of their target mRNAs, we determined the expression levels of target mRNAs by qRT-PCR. Indeed, the abundance of most target mRNAs was elevated in the *du13* and Y6 mutants compared to their wild types (Figures 7c and S12c; Table S4). Collectively, these findings indicate that Du13 is involved in the proper processing of pri-mRNAs.

To investigate potential mechanisms by which Du13 might affect miRNA processing, we performed a Y2H assay and determined that Du13 interacted with the key component of the miRNA processing complex, Hyponastic Leaves 1 (OsHYL1, *LOC_Os11g01869*; Figure S10a). Further BiFC and Co-IP assays are under the way to verify the interaction between Du13 and OsHYL1.

Discussion

Du13 is a novel splicing factor affecting amylose biosynthesis in rice endosperm

In this study, we report the isolation and characterization of the novel *dull* mutant, *du13*. In developing seeds, *du13* accumulated amylose in a temporal pattern similar to that of the wildtype but at a dramatically slower rate (Figure S2d), which correlated with the decrease in seed AC, OsGBSSI abundance, and activity (Figures 1d, 2h, 3c, d). Lower AC in *du13* endosperm was apparent at 5 DAF (Figure S2d, e), indicating that Du13 may function from the very early stages of endosperm development, when starch biosynthesis is initiated, in agreement with the high expression of *Du13* at this stage (Figure S6b, c).

The *du13* mutant affected the splicing of the Wx^b pre-mRNA but not overall transcript levels in developing endosperm (Figure 3e–h). Indeed, the abundance of unspliced Wx^b transcripts rose in *du13* endosperm, while spliced transcripts accumulated to lower levels (Figures 3g and 4e). These observations are distinct from the *du1* and *du2* mutants, in which the levels of unspliced Wx^b transcripts are comparable to those of the wild type, while spliced Wx^b transcripts are much less abundant (Isshiki *et al.*, 2000). In the *du3* mutant, the abundance of both unspliced and spliced Wx^b transcripts was reduced (Isshiki *et al.*, 2008).

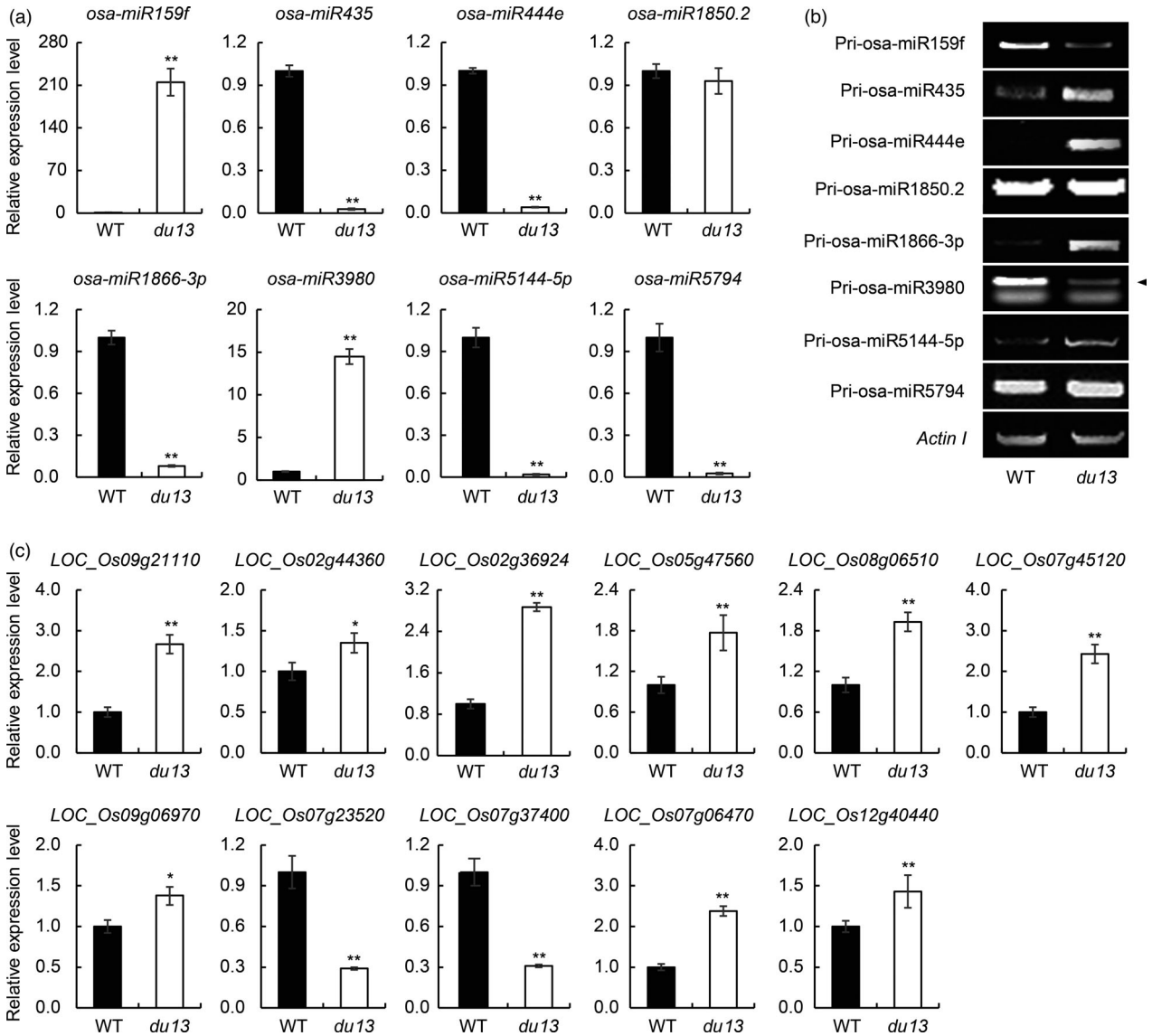

Figure 7 Analysis of expression levels for selected miRNAs, pri-miRNA transcripts, and miRNA target genes in the wild type and *du13*. (a) qRT-PCR analysis of differentially expressed miRNAs identified from miRNA-seq analysis. U6 snRNA was used as an internal control. The levels of these miRNAs in the wildtype (WT) were set to 1. Values are means ± SD (n = 3). (b) Abundance of pri-miRNAs in developing WT and *du13* endosperm at 10 DAF. The arrowhead indicates the specific band. (c) Relative expression levels of the target genes of osa-miR1866-3p (*LOC_Os09g21110* and *LOC_Os02g44360*), osa-miR435 (*LOC_Os02g44360*), osa-miR444e (*LOC_Os02g36924*, *LOC_Os05g47560*, *LOC_Os08g06510*, *LOC_Os07g45120*, and *LOC_Os09g06970*), osa-miR5144-5p (*LOC_Os07g23520*, *LOC_Os07g37400*, *LOC_Os02g44360*, *LOC_Os07g06470*, and *LOC_Os12g40440*), and osa-miR5794 (*LOC_Os09g06970*). Transcript levels in the WT were set to 1. *Actin I* was used as an internal control in (b) and (c). Values are means ± SD (n = 3). $*P < 0.05$, $**P < 0.01$, as determined by Student's t-test. *LOC_Os09g21110* encodes leucyl-tRNA synthetase; *LOC_Os02g44360* encodes scarecrow transcription factor family; *LOC_Os02g36924* encodes OsMADS27; *LOC_Os05g47560* encodes serine/threonine-protein kinase; *LOC_Os08g06510* encodes C3HC4-type zinc-finger protein; *LOC_Os07g45120* encodes expressed protein; *LOC_Os09g06970* encodes transport protein particle component (TRAPP) domain containing protein; *LOC_Os07g23520* encodes expressed protein; *LOC_Os07g37400* encodes F-box domain containing protein OsFBX257; *LOC_Os07g06470* encodes nuclear transcription factor Y subunit (NF-Y); *LOC_Os12g40440* encodes lipoate-protein ligase B.

Therefore, Du13 may have distinct effects on Wx^b splicing. In addition, Du13 enhanced the splicing efficiency of Wx^b at both cryptic sites, though preferentially at site 1 (Figure 4d), whereas Wx^b transcripts spliced at both sites were equally affected in *du1* or *du2* (Isshiki *et al.*, 2000). Moreover, like *du2* (Isshiki *et al.*, 2000), *du13* had minimal effects on AC in pollen grains (Figure 3a, b), reflecting its tissue-specific effects.

The splicing of transcripts for genes encoding starch biosynthetic enzymes, such as *starch branching enzyme I* (*BEI*), was affected in *du13* (Figure 6e; Table S3), in contrast to *du1*, *du2*, and *du3* (Isshiki *et al.*, 2000; Zeng *et al.*, 2007). Moreover, transcripts of many important splicing factor genes, such as *U2 auxiliary factor* (*U2AF*), and some miRNA biogenesis component genes, such as *DRB-2* (*double-stranded RNA-binding motif containing protein-2*), also showed altered AS profiles in *du13* (Figure 6e; Table S3). However, we observed no significant changes in BEI abundance and the levels of *DRB-2* transcripts (Figures S8c and S9g), which was consistent with a previous study

(Wang *et al*., 2019), implicating that the effects of altered splicing on the expression of protein-coding genes might be relatively weak. In summary, we saw more genes with intron retention in the *du13* mutant (Figure 6a). The first and last introns appeared to be more sensitive to loss of Du13 activity than internal introns (Figure 6b). In addition, alternative 5′ and 3′ splice site selection by du13 greatly increased within the first intron (Figure 6c, d), suggesting that Du13 might affect splice site choice mostly within the first intron, similar to SE and Arabidopsis CBPs (Raczynska *et al*., 2009, 2014).

Isshiki *et al*. (2000) proposed that Du1 (OsCBP20) and Du2 may be essential for recognizing the two weak splice sites activated in Wx^b exon 1 and stabilizing the spliceosomes assembled at both sites. Here, our data suggest that Du13 and OsCBC (OsCBP20 and OsCBP80) may coordinately influence splicing of Wx^b intron 1 (Figure 5), although the mechanistic details have not been resolved. In mammals, the CBC is essential for co-transcriptional spliceosome assembly via interaction with the U4/U6·U5 tri-snRNP (small nuclear ribonucleoprotein; Pabis *et al*., 2013). In *Arabidopsis*, SE colocalizes and interacts with U1 snRNP auxiliary proteins (Knop *et al*., 2017). We also determined that Du13 interacted with the splicing factor RSp29 in nuclear speckles (Figure S11d) where splicing factors are enriched (Fang and Spector, 2007). As we detected no interaction between Du1 and Du13 or OsCBC (Figure S10), further investigations into the detailed mechanism of Wx^b transcript splicing are still required. Notably, *du13* grains displayed a relatively soft and elastic texture compared to the wild-type Koshihikari, an elite *japonica* variety from Japan (Figure S2g; Table S2). The eating quality of *du13* was also better than that of Wuyujing 3, a well-known high-quality rice in Jiangsu, China (Table S5). Therefore, the *du13* mutant may contribute to in the improvement of rice quality.

Du13 is involved in miRNA biogenesis

The abundance of several mature miRNAs was reduced in *du13* endosperm (Figure 7a; Table S4). Of them, osa-miR435 was reported to be differentially expressed during rice grain filling (Yi *et al*., 2013). Many miRNAs including osa-miR435 are significantly upregulated from 5 to 7 DAF in rice grains, when a rapid increase in grain weight occurs (Wang *et al*., 2013; Yi *et al*., 2013). Moreover, the levels of osa-miR435, osa-miR444e, osa-miR1850.2 and osa-miR1866-3p are higher in superior spikelets compared to inferior spikelets, which show a slower grain-filling rate and a lower grain weight relative to superior spikelets (Peng *et al*., 2011). Hence, these results indicated the positive regulatory roles played by these miRNAs in grain filling. Many of their predicted target genes encoded transcription factors (Table S4). For instance, osa-miR444 was predicted to target MADS-box genes (Yi *et al*., 2013) that are considered necessary for rice ovule and seed development (Duan *et al*., 2005). The MADS gene (*LOC_Os02g36924*) displayed a higher expression level due to the lower abundance of osa-miR444e in *du13* endosperm (Figure 7a, c; Table S4). The constitutive co-expression of the two Arabidopsis MADS-box genes *SHATTERPROOF1* (*SHP1*) and *SHP2* resulted in plants with smaller fruits (Liljegren *et al*., 2000). Hence the higher expression of the MADS gene might contribute to the smaller and lighter grains of *du13* (Figure S1j–m; Table S1). Collectively, these results might at least in part explain the slow grain-filling rate and reduced grain weight in the *du13* mutant (Figure S1j–m; Table S1).

F-box genes, targeted by osa-miR1850.2, osa-miR1866-3p and osa-miR5144-5p (Table S4), have been shown to regulate grain size and plant architecture, particularly panicle architecture (Chen *et al*., 2013b; Duan *et al*., 2012; Li *et al*., 2011; Piao *et al*., 2009). Knockdown of the *F-box Kelch repeat protein* (*FBK*) gene *OsFBK12* produced smaller and lighter grains. *OsFBK12* expression levels also influenced plant height and panicle architecture including panicle length (Chen *et al*., 2013b). Moreover, mutations in the F-box gene *LARGER PANICLE* (*LP*) resulted in altered grain size, higher plant height, increased grain number per panicle and decreased tiller number (Li *et al*., 2011). We noticed altered expression levels for F-box genes (*LOC_Os07g37400*, *LOC_Os07g03100*, and *LOC_Os01g48250*) in *du13* (Figure 7c; Table S4), which might contribute to the pleiotropic phenotypes seen in *du13* plants, including reduced grain size and increased plant height (Figure S1a, j–l; Table S1). Additionally, osa-miR5144-5p is predicted to target transcripts for a nuclear transcription factor Y gene (NF-Y, *LOC_Os07g06470*), while both osa-miR444e and osa-miR5794 target a gene encoding a transport protein particle component (TRAPP, *LOC_Os09g06970*; Figure 7c; Table S4), which are required for shoot growth (Garcia *et al*., 2020; Sun *et al*., 2016). The higher expression of NF-Y and TRAPP in *du13* might contribute to the increased plant height of *du13* (Figure S1a; Table S1). Therefore, Du13 is required for the accumulation of important miRNAs critical to rice plant and grain development. We noted here that Du13 interacted with OsHYL1, a key component of the miRNA processing complex (Figure S10a), which might affect the cleavage of pri-miRNAs (Dong *et al*., 2008).

Previous studies have shown that many mutants of genes required for pre-mRNA splicing also exhibit defects in miRNA production (Chaabane *et al*., 2013; Kim *et al*., 2008; Laubinger *et al*., 2008). Indeed, pre-mRNA splicing and miRNA processing share many factors, including SE, CBPs, Stabilized 1 (STA1) and the Modifier of snc1,4 (MOS4)-associated complex (MAC; Chaabane *et al*., 2013; Jia *et al*., 2017; Kim *et al*., 2008; Laubinger *et al*., 2008; Li *et al*., 2018a; Zhang *et al*., 2013, 2014b). Moreover, important factors linked to spliceosomal function also appear to regulate both alternative pre-mRNA splicing and miRNA biogenesis, including SE, CBPs, STA1, MAC, Glycine-rich RNA-binding Protein 7 (AtGRP7), Increased Level of Polyploidy1-1D (ILP1), NTC-Related Protein 1 (NTR1), Tho Complex Subunit2 (THOC2), Sickle (SIC), Small1 (SMA1), High Osmotic Stress Gene Expression 5 (HOS5), FIERY2/RNAP II CTD phosphatase-like 1 (CPL1), RS40 and RS41 (Chaabane *et al*., 2013; Chen *et al*., 2013a, 2015; Francisco-Mangilet *et al*., 2015; Jia *et al*., 2017; Kim *et al*., 2008; Köster *et al*., 2014; Laubinger *et al*., 2008; Li *et al*., 2018a, 2018b; Manavella *et al*., 2012; Wang *et al*., 2019; Zhan *et al*., 2012; Zhang *et al*., 2013, 2014b). The significance of direct communication between the spliceosome and the miRNA biogenesis machinery in miRNA production has also been verified (Bielewicz *et al*., 2013; Knop *et al*., 2017; Schwab *et al*., 2013; Yan *et al*., 2012). Our results showed that Du13 also plays dual roles in alternative pre-mRNA splicing and miRNA biogenesis, confirming an evolutionarily conserved link between pre-mRNA splicing and microRNA biogenesis in land plants. Notably, Du1 is homologous to the pre-mRNA splicing factor STA1 (Chaabane *et al*., 2013; Zeng *et al*., 2007). It will thus be interesting to examine the abundance of miRNAs in the *du1*, *du2* and *du3* mutants.

The complicated function of Du13 in rice

SE homologs are highly conserved in yeast, plants, and animals (Wilson *et al*., 2008). They may have arisen early in evolution and

served a basic cellular function. Null alleles of SE homologs confer embryonic lethality in *Arabidopsis*, fission yeast (*Schizosaccharomyces pombe*), fruit fly (*Drosophila melanogaster*), zebrafish (*Danio rerio*) and mouse (*Mus musculus*; Amsterdam *et al*., 2004; Golling *et al*., 2002; Kim *et al*., 2010; Lobbes *et al*., 2006; Oh *et al*., 2003; Wilson *et al*., 2008). Most eukaryotic genomes encode a single *SE* homolog, whereas monocot genomes harbour multiple *SE* homologs (Figure S5a). As ZOS2-03 interacted with Du13 and OsCBC, ZOS2-03 might play a role similar to that of Du13 (Figures 5b and S13).

Like SE, Du13 may exert dual roles in pre-mRNA splicing and pri-miRNA processing in rice (Figure 8; Laubinger *et al*., 2008). Increasing evidence also suggests that SE is a multifunctional protein, playing an important role in epigenetic regulation of gene expression (Christie and Carroll, 2011; Ma *et al*., 2018; Wang *et al*., 2018). Whether Du13 has similar epigenetic regulatory roles in rice, is an exciting research topic to explore in the future.

Experimental procedures

Plant materials

The *du13* mutant was identified from an *N*-methyl-*N*-nitrosourea-induced M_2 population of the *japonica* rice cv. Koshihikari. *du13* was backcrossed to Koshihikari for genetic analysis. An F_2 population was derived from a cross between *du13* and the *indica* cv. Nanjing 11 for mapping. All plants were grown in an experimental field plot at Nanjing Agricultural University under natural conditions.

Microscopy

Scanning electron microscopy (SEM) was performed according to a previous report (Kang *et al*., 2005). Samples were examined using a Hitachi S-3400N scanning electron microscope. For the observation of compound starch granules, semi-thin sections (1 μm) were prepared as previously described (Peng *et al*., 2014). Semi-thin sections were stained with I_2-KI and examined with a Nikon ECLIPSE80i light microscope.

Physicochemical properties of rice grains

Mature rice grains were dehulled and ground into fine flour. The contents of amylose, lipid, total starch and protein, together with amylopectin chain-length distribution, were measured as previously described (Han *et al*., 2012). The starch pasting properties were determined as previously (Peng *et al*., 2014). Comprehensive taste evaluations of cooked rice were performed as previously described (Champagne *et al*., 1999).

Map-based cloning of the *du13* mutation

A total of 695 individuals with dull endosperm were selected from the F_2 mapping population. Over 180 genome-wide polymorphic SSR markers were used in preliminary mapping. For the fine-mapping of *Du13*, new genetic markers were developed by comparing the genomic sequences of *japonica* cv. Nipponbare and *indica* cv. 93-11 (Table S6).

Generation of transgenic plants

To complement the *du13* mutant, the wild-type *Du13* cDNA sequence was inserted into the binary vector pCUbi1390 (*Du13* is driven by its native promoter). A CRISPR-Cas9 construct expressing a single guide RNA (sgRNA) targeting exon 8 of *Du13* was assembled to generate knock-out mutants in *Du13*. The two constructs were individually introduced into *du13*, Nipponbare or Ningjing 7 calli by Agrobacterium (*Agrobacterium tumiefaciens*)-mediated *transformation as described previously (Hiei et al*., 1994).

Protein extraction and immunoblotting

Total protein extraction and immunoblot analysis were performed as previously described (Crofts *et al*., 2015; Wang *et al*., 2010). Polyclonal antibodies against Du13 and starch biosynthetic enzymes were produced in rabbits by Yingji Biotech (http://www.immunogen.com.cn/). Anti-HSP82 antibodies were purchased from Beijing Protein Innovation (AbM51099-31-PU).

Phylogenetic analysis

The neighbour-joining tree was generated using MEGA 5.0 software (http://www.megasoftware.net) by the bootstrap method (1000 replicates; Tamura *et al*., 2011). The amino acid sequences of Du13 homologs were retrieved on the National Center for Biotechnology Information (NCBI, http://www.ncbi.nlm.nih.gov) and aligned using ClustalX (http://www.clustal.org).

RNA extraction, RT-PCR, and qRT-PCR analysis

Total RNA was extracted using an RNAprep pure plant kit (Tiangen Co., Beijing, China). One microgram of total RNA was then reverse transcribed in a 20-μL reaction using PrimeScript II Reverse Transcriptase (TaKaRa) with oligo(dT_{18}) primers. Levels of pri-miRNAs were measured according to a previously described method (Juarez *et al*., 2004; Yang *et al*., 2006). qRT-PCR was performed with the SYBR Premix Ex Taq™ Kit (TaKaRa). *Actin I* was used as an internal control. Primers used are listed in Table S6.

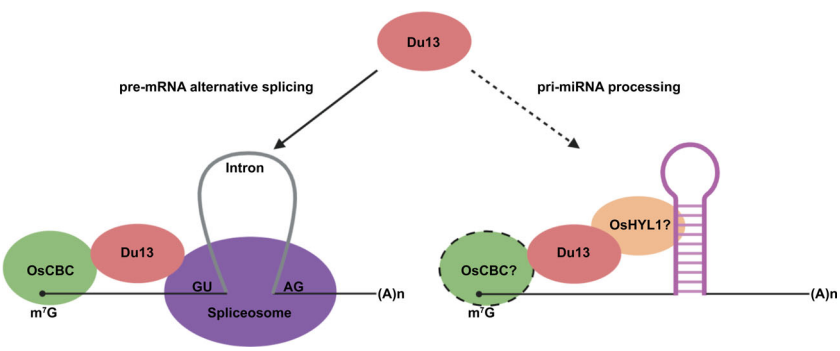

Figure 8 A model for the functions of Du13 in pre-mRNA splicing and pri-miRNA processing. Du13 interacts with spliceosome components and coordinates with OsCBC to influence pre-mRNA alternative splicing. Du13 also plays a role in miRNA biogenesis probably by interacting with OsHYL1. The role of OsCBC in miRNA biogenesis awaits further investigation.

Subcellular localization

The *Du13* cDNA was cloned in-frame and upstream of *GFP* in the pAN580-GFP vector (Peng *et al*., 2014). The resulting construct was transfected into rice protoplasts according to previously described protocols (Chen *et al*., 2006). *du13*, *ZOS2-03*, *ZOS8-11*, *OsCBP20*, *OsCBP80*, and *RSp29* cDNAs were similarly cloned into the binary vector, pCAMBIA1305-GFP (driven by the CaMV 35S promoter), before transient infiltration in *N. benthamiana* leaves (Waadt and Kudla, 2008). Confocal imaging analysis was performed using a Zeiss LSM710 confocal microscope.

Enzyme activity assays

Developing endosperm collected at 10 days after fertilization (DAF) was homogenized in 10-fold volume of a solution consisting of 50 mM HEPES-NaOH (pH 7.4), 50 mM 2-mercaptoethanol, 2 mM $MgCl_2$, and 12.5% (v/v) glycerol (Nishi *et al*., 2001). After centrifugation, the supernatant was used to assay the activity of soluble starch synthases, while the pellet was resuspended in 1 mL of the above solution for GBSSI activity assay (Nakamura *et al*., 1989).

Y2H and transcriptional activity assays

Full-length *Du13* and *ZOS2-03* cDNAs were cloned into both pGBKT7 and pGADT7 vectors. *Du1* and truncated *Du13* cDNAs were cloned into the pGBKT7 vector, and *OsCBP20*, *OsCBP80*, *HYL1*, *ZOS8-11*, *RSp29*, *RSZp23*, and two homologs of *RSZp23* (*RSZp21a* and *RSZp21b*) cDNAs were cloned into the pGADT7 vector. Yeast strain AH109 was co-transformed with various combinations of plasmids, according to the manufacturer's instructions (Clontech, Mountain View, CA). Interactions were assayed using synthetic define (SD) –Leu–Trp–His–Ade medium.

The BD-Du13 construct was transformed into AH109 and transcriptional activity was assayed on SD –Trp–His–Ade medium.

Transient assays using rice protoplasts

Du13, *du13*, and *ZOS2-03* cDNAs were cloned into the pAN580-GFP vector (with its *GFP* fragment removed) to produce constructs driven by the CaMV 35S promoter. These plasmids were mixed with rice protoplasts together with a Wx^b-*gus* plasmid (Isshiki *et al*., 2006). The Wx^b-*gus* plasmid was also transfected into wild-type and *du13* protoplasts. GUS activity and RT-PCR analyses were performed as previously described (Isshiki *et al*., 2006).

BiFC assay

Full-length *Du13*, *OsCBP20,* and *ZOS2-03* cDNAs were introduced into both the p2YN and p2YC (encoding each half of eYFP) vectors (Zheng *et al*., 2015). *Du1* and *RSp29* were cloned into the p2YN vector, and *OsCBP80* was cloned into the p2YC vector. BiFC assays were conducted in *N. benthamiana* leaf epidermal cells, as described previously (Peng *et al*., 2014).

Co-IP assay

Coding sequences of *Du13* and *ZOS2-03* were introduced into the binary vector pCAMBIA1300-221-Flag and transformed into Agrobacterium strain EHA105. The plasmid for the subcellular localization of ZOS2-03 and plasmids for BiFC assays of OsCBP20 and OsCBP80 (as HA fusions), were also used in the Co-IP assay. *N. benthamiana* leaves were co-infiltrated with different combinations of plasmids and collected at 48 h after infiltration (Qiao *et al*., 2017). Anti-GFP antibodies (Medical Biological Laboratories (MBL, M048-3), anti-HA antibodies (MBL, M180-7), anti-Flag antibodies (Sigma-Aldrich, A8592), and anti-Flag agarose (MBL, M185-10) were used in Co-IP experiments.

mRNA-seq and miRNA-seq

Total RNA was extracted from immature rice grains at 10 DAF removed of the hull, pericarp, and embryo. Illumina sequencing libraries for mRNA-seq and miRNA-seq were prepared following the manufacturer's instructions and then sequenced on a HiSeq platform. The raw reads were processed with Hisat2 and StringTie, followed by the software rMATS (Shen *et al*., 2014) to classify alternative splicing profiles in each sample. For miRNA-seq, DEGseq was employed to identify differentially expressed miRNAs. To validate differentially expressed miRNAs obtained from miRNA-seq, miRNA extraction, RT-PCR, and qRT-PCR analyses were performed according to the manufacturer's instructions (Tiangen Biotech, Beijing, China). U6 snRNA was used as an internal reference.

Acknowledgements

This research was supported by the National Key R&D Program of China (2021YFF1000200), the National Transform Science and Technology Program (2016ZX08001006), the National Natural Science Foundation Integration Project (91935301), the Jiangsu Science and Technology Development Program (BE2018398), the Jiangsu Province Agriculture Independent Innovation Fund Project (SCX(19)1079), the Fundamental Research Funds for the Central Universities (KYTZ201601), the Key Laboratory of Biology, Genetics and Breeding of Japonica Rice in the Mid-lower Yangtze River, Ministry of Agriculture and Rural Affairs, China, and the Jiangsu Collaborative Innovation Center for Modern Crop Production, China.

Conflict of interests

The authors declare no competing interests.

Author contributions

YC, WWZ and JMW designed the experiments. WWC, XGC, JM, XJT and JZ screened the mutant materials. PW and FK mapped *du13*. YC, YSF, ZZS, JHX, JJ, HGY, XYG and YXW performed experiments. XMY, JC, XL and JHX constructed some vectors. YQB, LJ, HYW and JMW directed the project. YC, WWZ, YSF, and ZZS contributed equally to this work.

References

Aluko, G., Martinez, C., Tohme, J., Castano, C., Bergman, C. and Oard, J.H. (2004) QTL mapping of grain quality traits from the interspecific cross *Oryza sativa* x *O. glaberrima*. *Theoret. Appl. Genet.* **109**, 630–639.

Amsterdam, A., Nissen, R.M., Sun, Z., Swindell, E.C., Farrington, S. and Hopkins, N. (2004) Identification of 315 genes essential for early zebrafish development. *Proc. Natl Acad. Sci. USA,* **101**(35), 12792–12797.

Bielewicz, D., Kalak, M., Kalyna, M., Windels, D., Barta, A., Vazquez, F., Szweykowska-Kulinska, Z. *et al*. (2013) Introns of plant pri-miRNAs enhance miRNA biogenesis. *EMBO Rep.* **14**, 622–628.

Cai, X.L., Wang, Z.Y., Xing, Y.Y., Zhang, J.L. and Hong, M.M. (1998) Aberrant splicing of intron 1 leads to the heterogeneous 5' UTR and decreased expression of *waxy* gene in rice cultivars of intermediate amylose content. *Plant J.* **14**, 459–465.

Chaabane, S.B., Liu, R.Y., Chinnusamy, V., Kwon, Y., Park, J.H., Kim, S.Y., Zhu, J.K. *et al*. (2013) STA1, an Arabidopsis pre-mRNA processing factor 6 homolog, is a new player involved in miRNA biogenesis. *Nucleic Acids Res.* **41**, 1984–1997.

Champagne, E.T., Bett, K.L., Vinyard, B.T., McClung, A.M., Barton, F.E., Moldenhauer, K., Linscombe, S. *et al*. (1999) Correlation between cooked rice texture and Rapid Visco Analyser measurements. *Cereal Chem.* **76**(5), 764–771.

Chen, S.B., Tao, L., Zeng, L.R., Vega-Sanchez, M.E., Umemura, K. and Wang, G.L. (2006) A highly efficient transient protoplast system for analyzing defence gene expression and protein-protein interactions in rice. *Mol. Plant Pathol.* **7**, 417–427.

Chen, T., Cui, P., Chen, H., Ali, S., Zhang, S. and Xiong, L. (2013a) A KH-domain RNA-binding protein interacts with FIERY2/CTD phosphatase-like 1 and splicing factors and is important for pre-mRNA splicing in Arabidopsis. *PLoS Genet.* **9**, e1003875.

Chen, T., Cui, P. and Xiong, L. (2015) The RNA-binding protein HOS5 and serine/arginine-rich proteins RS40 and RS41 participate in miRNA biogenesis in Arabidopsis. *Nucleic Acids Res.* **43**, 8283–8298.

Chen, Y., Xu, Y., Luo, W., Li, W., Chen, N., Zhang, D. and Chong, K. (2013b) The F-box protein OsFBK12 targets OsSAMS1 for degradation and affects pleiotropic phenotypes, including leaf senescence, in rice. *Plant Physiol.* **163**, 1673–1685.

Christie, M. and Carroll, B.J. (2011) *SERRATE* is required for intron suppression of RNA silencing in Arabidopsis. *Plant Signal. Behav.* **6**, 2035–2037.

Crofts, N., Abe, N., Oitome, N.F., Matsushima, R., Hayashi, M., Tetlow, I.J., Emes, M.J. *et al*. (2015) Amylopectin biosynthetic enzymes from developing rice seed form enzymatically active protein complexes. *J. Exp. Bot.* **66**, 4469–4482.

Dong, Z., Han, M.H. and Fedoroff, N. (2008) The RNA-binding proteins HYL1 and SE promote accurate *in vitro* processing of pri-miRNA by DCL1. *Proc. Natl Acad. Sci. USA,* **105**, 9970–9975.

Duan, K., Luo, Y.H., Luo, D., Xu, Z.H. and Xue, H.W. (2005) New insights into the complex and coordinated transcriptional regulation networks underlying rice seed development through cDNA chip-based analysis. *Plant Mol. Biol.* **57**, 785–804.

Duan, Y.L., Li, S.P., Chen, Z.W., Zheng, L.L., Diao, Z.J., Zhou, Y.C., Lan, T. *et al*. (2012) *Dwarf and deformed flower 1*, encoding an F-box protein, is critical for vegetative and floral development in rice (*Oryza sativa* L.). *Plant J.* **72**, 829–842.

Fang, Y. and Spector, D.L. (2007) Identification of nuclear dicing bodies containing proteins for microRNA biogenesis in living *Arabidopsis* plants. *Curr. Biol.* **17**, 818–823.

Frances, H., Bligh, J., Larkin, P.D., Roach, P.S., Jones, C.A., Fu, H. and Park, W.D. (1998) Use of alternate splice sites in granule-bound starch synthase mRNA from low-amylose rice varieties. *Plant Mol. Biol.* **38**, 407–415.

Francisco-Mangilet, A.G., Karlsson, P., Kim, M.H., Eo, H.J., Oh, S.A., Kim, J.H., Kulcheski, F.R. *et al*. (2015) THO2, a core member of the THO/TREX complex, is required for microRNA production in Arabidopsis. *Plant J.* **82**, 1018–1029.

Garcia, V., Xu, S.L., Ravikumar, R., Wang, W.F., Elliott, L., Efren, G., Fesenko, M. *et al*. (2020) TRIPP is a plant-specific component of the Arabidopsis TRAPPII membrane trafficking complex with important roles in plant development. *Plant Cell*, **32**, 2424–2443.

Golling, G., Amsterdam, A., Sun, Z.X., Antonelli, M., Maldonado, E., Chen, W.B., Burgess, S. *et al*. (2002) Insertional mutagenesis in zebrafish rapidly identifies genes essential for early vertebrate development. *Nat. Genet.* **31**, 135–140.

Grigg, S.P., Canales, C., Hay, A. and Tsiantis, M. (2005) *SERRATE* coordinates shoot meristem function and leaf axial patterning in *Arabidopsis*. *Nature*, **437**, 1022–1026.

Han, X.H., Wang, Y.H., Liu, X., Jiang, L., Ren, Y.L., Liu, F., Peng, C. *et al*. (2012) The failure to express a protein disulphide isomerase-like protein results in a floury endosperm and an endoplasmic reticulum stress response in rice. *J. Exp. Bot.* **63**, 121–130.

Hiei, Y., Ohta, S., Komari, T. and Kumashiro, T. (1994) Efficient transformation of rice (*Oryza sativa* L.) mediated by *Agrobacterium* and sequence analysis of the boundaries of the T-DNA. *Plant J.* **6**, 271–282.

Hirano, H.Y., Eiguchi, M. and Sano, Y.A. (1998) Single-base change altered the regulation of the *Waxy* gene at the posttranscriptional level during the domestication of rice. *Mol. Biol. Evol.* **15**, 978–987.

Isshiki, M., Matsuda, Y., Takasaki, A., Wong, H.L., Satoh, H. and Shimamoto, K. (2008) *Du3*, a mRNA cap-binding protein gene, regulates amylose content in Japonica rice seeds. *Plant Biotechnol.* **25**, 483–487.

Isshiki, M., Morino, K., Nakajima, M., Okagaki, R.J., Wessler, S.R., Izawa, T. and Shimamoto, K. (1998) A naturally occurring functional allele of the rice *waxy* locus has a GT to TT mutation at the 5′ splice site of the first intron. *Plant J.* **15**, 133–138.

Isshiki, M., Nakajima, M., Satoh, H. and Shimamoto, K. (2000) *dull*: rice mutants with tissue-specific effects on the splicing of the *waxy* pre-mRNA. *Plant J.* **23**, 451–460.

Isshiki, M., Tsumoto, A. and Shimamoto, K. (2006) The Serine/Arginine-rich protein family in rice plays important roles in constitutive and alternative splicing of pre-mRNA. *Plant Cell*, **18**, 146–158.

Jia, T.R., Zhang, B.L., You, C.J., Zhang, Y., Zeng, L.P., Li, S.J., Johnson, K.C.M. *et al*. (2017) The Arabidopsis MOS4-associated complex promotes microRNA biogenesis and precursor messenger RNA splicing. *Plant Cell*, **29**, 2626–2643.

Juarez, M.T., Kui, J.S., Thomas, J., Heller, B.A. and Timmermans, M.C.P. (2004) microRNA-mediated repression of *rolled leaf1* specifies maize leaf polarity. *Nature*, **428**, 84–88.

Kang, H.G., Park, S., Matsuoka, M. and An, G. (2005) White-core endosperm *floury endosperm-4* in rice is generated by knockout mutations in the C4-type pyruvate orthophosphate dikinase gene (OsPPDKB). *Plant J.* **42**, 901–911.

Kaushik, R.P. and Khush, G.S. (1991) Endosperm mutants in rice: gene expression in japonica and Indica backgrounds. *Cereal Chem.* **68**, 487–491.

Kierzkowski, D., Kmieciak, M., Piontek, P., Wojtaszek, P., Szewykowska-Kulinska, Z. and Jarmolowski, A. (2009) The Arabidopsis CBP20 targets the cap-binding complex to the nucleus, and is stabilized by CBP80. *Plant J.* **59**, 813–823.

Kim, D.U., Hayles, J., Kim, D., Wood, V., Park, H.O., Won, M., Yoo, H.S. *et al*. (2010) Analysis of a genome-wide set of gene deletions in the fission yeast Schizosaccharomyces pombe. *Nat. Biotechnol.* **28**, 617–623.

Kim, S., Yang, J.Y., Xu, J., Jang, I.C., Prigge, M.J. and Chua, N.H. (2008) Two cap-binding proteins CBP20 and CBP80 are involved in processing primary microRNAs. *Plant Cell Physiol.* **49**, 1634–1644.

Kiswara, G., Lee, J.H., Hur, Y.J., Cho, J.H., Lee, J.Y., Kim, S.Y., Sohn, Y.B. *et al*. (2014) Genetic analysis and molecular mapping of low amylose gene *du12(t)* in rice (*Oryza sativa* L.). *Theoret. Appl. Genet.* **127**, 51–57.

Knop, K., Stepien, A., Barciszewska-Pacak, M., Taube, M., Bielewicz, D., Michalak, M., Borst, J.W. *et al*. (2017) Active 5′ splice sites regulate the biogenesis efficiency of Arabidopsis microRNAs derived from intron-containing genes. *Nucleic Acids Res.* **45**, 2757–2775.

Köster, T., Meyer, K., Weinholdt, C., Smith, L.M., Lummer, M., Speth, C., Grosse, I. *et al*. (2014) Regulation of pri-miRNA processing by the hnRNP-like protein AtGRP7 in Arabidopsis. *Nucleic Acids Res.* **42**, 9925–9936.

Laubinger, S., Sachsenberg, T., Zeller, G., Busch, W., Lohmann, J.U., Rätsch, G. and Weigel, D. (2008) Dual roles of the nuclear cap binding complex and SERRATE in pre-mRNA splicing and microRNA processing in *Arabidopsis thaliana*. *Proc. Natl Acad. Sci. USA*, **105**, 8795–8800.

Li, M., Tang, D., Wang, K.J., Wu, X.R., Lu, L.L., Yu, H.X., Gu, M.H. *et al*. (2011) Mutations in the F-box gene *LARGER PANICLE* improve the panicle architecture and enhance the grain yield in rice. *Plant Biotechnol. J.* **9**, 1002–1013.

Li, S.J., Liu, K., Zhou, B.J., Li, M., Zhang, S.X., Zeng, L.R., Zhang, C. *et al*. (2018a) MAC3A and MAC3B, two core subunits of the MOS4-associated complex, positively influence miRNA biogenesis. *Plant Cell*, **30**, 481–494.

Li, S.J., Xu, R., Li, A.X., Liu, K., Gu, L.Q., Li, M., Zhang, H.R. *et al*. (2018b) SMA1, a homolog of the splicing factor Prp28, has a multifaceted role in miRNA biogenesis in Arabidopsis. *Nucleic Acids Res.* **46**, 9148–9159.

Liljegren, S.J., Ditta, G.S., Eshed, Y., Savidge, B., Bowman, J.L. and Yanofsky, M.F. (2000) *SHATTERPROOF* MADS-box genes control seed dispersal in *Arabidopsis*. *Nature*, **404**, 766–770.

Liu, L.L., Ma, X.D., Liu, S.J., Zhu, C.L., Jiang, L., Wang, Y.H., Shen, Y. *et al*. (2009) Identification and characterization of a novel *Waxy* allele from a Yunnan rice landrace. *Plant Mol. Biol.* **71**, 609–626.

Lobbes, D., Rallapalli, G., Schmidt, D.D., Martin, C. and Clarke, J. (2006) *SERRATE*: a new player on the plant microRNA scene. *EMBO Rep.* **7**, 1052–1058.

Ma, Z., Castillo-González, C., Wang, Z., Sun, D., Hu, X., Shen, X., Potok, M.E. *et al*. (2018) Arabidopsis serrate coordinates histone methyltransferases ATXR5/6 and RNA processing factor RDR6 to regulate transposon expression. *Dev. Cell*, **45**, 769–784.

Manavella, P.A., Hagmann, J., Ott, F., Laubinger, S., Franz, M., Macek, B. and Weigel, D. (2012) Fast-forward genetics identifies plant CPL phosphatases as regulators of miRNA processing factor HYL1. *Cell*, **151**, 859–870.

Nakamura, Y., Yuki, K., Park, S.Y. and Ohya, T. (1989) Carbohydrate metabolism in the developing endosperm of rice grains. *Plant Cell Physiol.* **30**, 833–839.

Nishi, A., Nakamura, Y., Tanaka, N. and Satoh, H. (2001) Biochemical and genetic analysis of the effects of amylose-extender mutation in rice endosperm. *Plant Physiol.* **127**, 459–472.

Oh, S.W., Kingsley, T., Shin, H.H., Zheng, Z., Chen, H.W., Chen, X., Wang, H. *et al*. (2003) A P-element insertion screen identified mutations in 455 novel essential genes in Drosophila. *Genetics*, **163**, 195–201.

Pabis, M., Neufeld, N., Steiner, M.C., Bojic, T., Shav-Tal, Y. and Neugebauer, K.M. (2013) The nuclear cap-binding complex interacts with the U4/U6·U5 tri-snRNP and promotes spliceosome assembly in mammalian cells. *RNA*, **19**, 1054–1063.

Peng, C., Wang, Y.H., Liu, F., Ren, Y.L., Zhou, K.N., Lv, J., Zheng, M. *et al*. (2014) *FLOURY ENDOSPERM6* encodes a CBM48 domain-containing protein involved in compound granule formation and starch synthesis in rice endosperm. *Plant J.* **77**, 917–930.

Peng, T., Lv, Q., Zhang, J., Li, J.Z., Du, Y.X. and Zhao, Q.Z. (2011) Differential expression of the microRNAs in superior and inferior spikelets in rice (*Oryza sativa*). *J. Exp. Bot.* **62**, 4943–4954.

Piao, R., Jiang, W., Ham, T.H., Choi, M.S., Qiao, Y., Chu, S.H., Park, J.H. *et al*. (2009) Map-based cloning of the *ERECT PANICLE 3* gene in rice. *Theoret. Appl. Genet.* **119**, 1497–1506.

Qiao, S.L., Sun, S.Y., Wang, L.L., Wu, Z.H., Li, C.X., Li, X.M., Wang, T. *et al*. (2017) The RLA1/SMOS1 transcription factor functions with OsBZR1 to regulate brassinosteroid signaling and rice architecture. *Plant Cell*, **29**, 292–309.

Raczynska, K.D., Simpson, C.G., Ciesiolka, A., Szewc, L., Lewandowska, D., McNicol, J., Szweykowska-Kulinska, Z. *et al*. (2009) Involvement of the nuclear cap-binding protein complex in alternative splicing in *Arabidopsis thaliana*. *Nucleic Acids Res.* **38**, 265–278.

Raczynska, K.D., Stepien, A., Kierzkowski, D., Kalak, M., Bajczyk, M., McNicol, J., Simpson, C.G. *et al*. (2014) The SERRATE protein is involved in alternative splicing in *Arabidopsis thaliana*. *Nucleic Acids Res.* **42**, 1224–1244.

Schwab, R., Speth, C., Laubinger, S. and Voinnet, O. (2013) Enhanced microRNA accumulation through stemloop-adjacent introns. *EMBO Rep.* **14**, 615–621.

Shen, S., Park, J.W., Lu, Z.X., Lin, L., Henry, M.D., Wu, Y.N., Zhou, Q. *et al*. (2014) rMATS: Robust and flexible detection of differential alternative splicing from replicate RNA-Seq data. *Proc. Natl Acad. Sci. USA*, **111**, E5593–E5601.

Sun, X.D., Ren, Y.Q., Zhang, X.Z., Lian, H.F., Zhou, S.M. and Liu, S.Q. (2016) Overexpression of a garlic nuclear factor Y (NF-Y) B gene, *AsNF-YB3*, affects seed germination and plant growth in transgenic tobacco. *Plant Cell, Tissue Organ Cult.* **127**, 513–523.

Tamura, K., Peterson, D., Peterson, N., Stecher, G., Nei, M. and Kumar, S. (2011) MEGA5: molecular evolutionary genetics analysis using maximum likelihood, evolutionary distance, and maximum parsimony methods. *Mol. Biol. Evol.* **28**, 2731–2739.

Waadt, R. and Kudla, J. (2008) *In planta* visualization of protein interactions using bimolecular fluorescence complementation (BiFC). *Cold Spring Harbor Protocols*, **2008**(4), pdb.prot4995.

Wang, J.L., Chen, S.S., Jiang, N., Li, N., Wang, X.Y., Li, Z.P., Li, X. *et al*. (2019) Spliceosome disassembly factors ILP1 and NTR1 promote miRNA biogenesis in *Arabidopsis thaliana*. *Nucleic Acids Res.* **47**, 7886–7900.

Wang, J.C., Xu, H., Zhu, Y., Liu, Q.Q. and Cai, X.L. (2013) OsbZIP58, a basic leucine zipper transcription factor, regulates starch biosynthesis in rice endosperm. *J. Exp. Bot.* **64**, 3453–3466.

Wang, Y.H., Ren, Y.L., Liu, X., Jiang, L., Chen, L.M., Han, X.H., Jin, M.N. *et al*. (2010) OsRab5a regulates endomembrane organization and storage protein trafficking in rice endosperm cells. *Plant J.* **64**, 812–824.

Wang, Z.Y., Ma, Z.Y., Castillo-González, C., Sun, D., Li, Y.J., Yu, B., Zhao, B.Y. *et al*. (2018) SWI2/SNF2 ATPase CHR2 remodels pri-miRNAs via Serrate to impede miRNA production. *Nature*, **557**, 516–521.

Wang, Z.Y., Wu, Z.L., Xing, Y.Y., Zheng, F.G., Guo, X.L., Zhang, W.G. and Hong, M.M. (1990) Nucleotide sequence of rice *waxy* gene. *Nucleic Acids Res.* **18**, 5898.

Wilson, M.D., Wang, D., Wagner, R., Breyssens, H., Gertsenstein, M., Lobe, C., Lu, X. *et al*. (2008) *ARS2* is a conserved eukaryotic gene essential for early mammalian development. *Mol. Cell Biol.* **28**, 1503–1514.

Yan, K., Liu, P., Wu, C.A., Yang, G.D., Xu, R., Guo, Q.H., Huang, J.G. *et al*. (2012) Stress-induced alternative splicing provides a mechanism for the regulation of microRNA processing in *Arabidopsis thaliana*. *Mol. Cell*, **48**, 521–531.

Yang, L., Liu, Z., Lu, F., Dong, A. and Huang, H. (2006) *SERRATE* is a novel nuclear regulator in primary microRNA processing in *Arabidopsis*. *Plant J.* **47**, 841–850.

Yi, R., Zhu, Z.X., Hu, J.H., Qian, Q., Dai, J.C. and Ding, Y. (2013) Identification and expression analysis of microRNAs at the grain filling stage in rice (*Oryza sativa* L.) via deep sequencing. *PLoS One*, **8**, e57863.

Zeng, D.L., Yan, M.X., Wang, Y.H., Liu, X.F., Qian, Q. and Li, J.Y. (2007) *Du1*, encoding a novel Prp1 protein, regulates starch biosynthesis through affecting the splicing of Wx^b pre-mRNAs in rice (*Oryza sativa* L.). *Plant Mol. Biol.* **65**, 501–509.

Zhan, X.Q., Wang, B.S., Li, H.J., Liu, R.Y., Kalia, R.K., Zhu, J.K. and Chinnusamy, V. (2012) Arabidopsis proline-rich protein important for development and abiotic stress tolerance is involved in microRNA biogenesis. *Proc. Natl Acad. Sci. USA,* **109**, 18198–18203.

Zhang, H., Duan, L., Dai, J.S., Zhang, C.Q., Li, J., Gu, M.H., Liu, Q.Q. *et al*. (2014a) Major QTLs reduce the deleterious effects of high temperature on rice amylose content by increasing splicing efficiency of *Wx* pre-mRNA. *Theoret. Appl. Gen.* **127**, 273–282.

Zhang, S.X., Liu, Y.H. and Yu, B. (2014b) PRL1, an RNA-binding protein, positively regulates the accumulation of miRNAs and siRNAs in Arabidopsis. *PLoS Genet.* **10**, e1004841.

Zhang, S.X., Xie, M., Ren, G.D. and Yu, B. (2013) CDC5, a DNA binding protein, positively regulates posttranscriptional processing and/or transcription of primary microRNA transcripts. *Proc. Natl Acad. Sci. USA,* **110**(43), 17588–17593.

Zheng, M., Wang, Y.H., Wang, Y.L., Wang, C.M., Ren, Y.L., Lv, J., Peng, C. *et al*. (2015) *DEFORMED FLORAL ORGAN1* (*DFO1*) regulates floral organ identity by epigenetically repressing the expression of *OsMADS58* in rice (*Oryza sativa*). *New Phytol.* **206**, 1476–1490.

Supporting information

Additional supporting information may be found online in the Supporting Information section at the end of the article.

Figure S1 Phenotypic analysis of the *du13* mutant.
Figure S2 Grain properties and physicochemical characteristics of starch in the *du13* mutant.
Figure S3 DNA and protein sequence alignments in the wild type and the mutants *du13* and Y6.
Figure S4 Characterization of homozygous *du13* knockout mutants and phenotypic analysis of transgenic grains.
Figure S5 Phylogenetic and functional domain analyses of Du13.
Figure S6 Expression analysis of *Du13* and subcellular localization of Du13.
Figure S7 Subcellular localization of du13, OsCBP20, OsCBP80, RSp29, ZOS2-03, and ZOS8-11.
Figure S8 Expression levels of starch biosynthesis-related genes.

Figure S9 Relative expression levels of *OsCBP20* and *OsCBP80* and interaction between OsCBP20 and OsCBP80.
Figure S10 Du1 does not interact with Du13 or OsCBC.
Figure S11 Interactions among Du13 homologs and SR proteins.
Figure S12 Expression analysis of selected miRNAs, pri-miRNA transcripts, and miRNA target genes in the Y6 mutant.
Figure S13 ZOS2-03 interacts with Du13 and OsCBC.
Table S1 Agronomic traits of the wild type (WT) and *du13*.
Table S2 Pasting properties of wild-type (WT) and *du13* endosperm starch.
Table S3 Changes in alternative splicing events in the *du13* mutant.
Table S4 miRNAs of reduced abundance and their target genes of altered expression in *du13* by miRNA-seq analysis.
Table S5 Eating quality of Wuyujing 3 and *du13* grains.
Table S6 Primers used in this study.